

Widely tunable, non-degenerate three-wave mixing microwave device operating near the quantum limit

N. Roch,¹ E. Flurin,¹ F. Nguyen,^{1,*} P. Morfin,¹ P. Campagne-Ibarcq,¹ M. H. Devoret,^{2,1,3} and B. Huard^{1,†}

¹*Laboratoire Pierre Aigrain, Ecole Normale Supérieure,*

CNRS (UMR 8551), Université P. et M. Curie,

Université D. Diderot 24, rue Lhomond, 75231 Paris Cedex 05, France

²*Collège de France, 11 Place Marcelin Berthelot, F-75231 Paris Cedex 05, France*

³*Department of Applied Physics, Yale University, PO Box 208284, New Haven, CT 06520-8284*

(Dated: February 22, 2012)

We present the first experimental realization of a widely frequency tunable, non-degenerate three-wave mixing device for quantum signals at GHz frequency. It is based on a new superconducting building-block consisting of a ring of four Josephson junctions shunted by a cross of four linear inductances. The phase configuration of the ring remains unique over a wide range of magnetic fluxes threading the loop. It is thus possible to vary the inductance of the ring with flux while retaining a strong, dissipation-free, and noiseless non-linearity. The device has been operated in amplifier mode and its noise performance has been evaluated by using the noise spectrum emitted by a voltage biased tunnel junction at finite frequency as a test signal. The unprecedented accuracy with which the crossover between zero-point-fluctuations and shot noise has been measured provides an upper-bound for the noise and dissipation intrinsic to the device.

PACS numbers:

Three-wave mixing devices, i.e. non-linear circuits converting power among three microwave signals, are key elements of analog information processing in the microwave domain[1]. However, they are based on dissipative components such as semiconductor diodes, or SIS tunnel junctions biased near the superconducting gap[2]. The loss of signal limits their operation and also introduces noise above the minimum required by quantum mechanics[3, 4]. A non-degenerate mixing device with noise close to that minimum level was demonstrated recently [5, 6]. However, the hysteresis preventing flux tunability for this 4-junction circuit severely limited possible applications to analog quantum signal processing. In this Letter, we show that by adding four inductances to the 4-junction loop, we can fully suppress the hysteresis and reach a 500MHz frequency tunability while operating close to the quantum limit. Our improvement of the device tunability by an order of magnitude is obtained without jeopardizing other advantages of non-degenerate 3-wave mixing.

An ideal non-degenerate three-wave mixing device in the microwave domain absorbs three signals at frequencies such that $\omega_X + \omega_Y = \omega_Z$ with complex amplitudes A_X^{in} , A_Y^{in} and A_Z^{in} , respectively, and reemits signals at the same frequencies with amplitudes A_X^{out} , A_Y^{out} and A_Z^{out} such that $|A_X^{out}|^2 + |A_Y^{out}|^2 + |A_Z^{out}|^2 = |A_X^{in}|^2 + |A_Y^{in}|^2 + |A_Z^{in}|^2$, that is without internal dissipation. The device can operate in two power amplification modes: i) the photon gain mode, for which $|A_Z^{in}|^2 \gg |A_X^{in}|^2, |A_Y^{in}|^2$ is the pump power providing the extra photon numbers in the re-emitted signals at frequencies ω_X and ω_Y , and ii) the pure up-conversion mode for which $|A_Y^{in}|^2 \gg |A_X^{in}|^2, |A_Z^{in}|^2$ is the pump power providing the energy difference between

photons at ω_Z and photons at ω_X . The Josephson Parametric Converter (JPC)[6], consisting of a ring of four Josephson junctions, can perform both functions. However, its operation has little tunability since the flux Φ_{ext} applied through the ring has to be adjusted in the close vicinity of the value $\Phi_0/2$, where $\Phi_0 = h/2e$ is the flux quantum. In the present work, we consider a more general 3-wave mixing device in which 4 linear inductances are cross-linking the ring-modulator like the spokes of a wheel (see Fig.1a). The hamiltonian of the ring is

$$H = -\frac{1}{2}E_J \sin(\varphi_{ext})\varphi_X\varphi_Y\varphi_Z + \frac{1}{2}(E_L/2 + E_J \cos \varphi_{ext})(\varphi_X^2 + \varphi_Y^2) + \frac{1}{2}(E_L/4 + E_J \cos \varphi_{ext})\varphi_Z^2 + O(\varphi_{X,Y,Z}^4) \quad (1)$$

where the three spatial mode amplitudes $\varphi_X = \varphi_1 - \varphi_3$, $\varphi_Y = \varphi_2 - \varphi_4$ and $\varphi_Z = \varphi_1 + \varphi_3 - \varphi_2 - \varphi_4$ are gauge-invariant, orthogonal linear combinations of the superconducting phases of the four nodes of the Josephson junction ring (Fig. 1b).

We will see below how these standing wave modes can be excited by the propagating mode amplitudes A_X^{in} , A_Y^{in} and A_Z^{in} and emit the amplitudes A_X^{out} , A_Y^{out} and A_Z^{out} . In the hamiltonian (1), $E_L = \varphi_0^2/L$ is the energy associated with each of the inductances L , and $E_J = \varphi_0^2/L_J^0$ is the Josephson energy of each tunnel junction. We also define the reduced flux quantum $\varphi_0 = \hbar/2e$ and the dimensionless flux $\varphi_{ext} = \Phi_{ext}/4\varphi_0$ threading each of the nominally identical 4 loops of the device. The first term of the hamiltonian is a pure 3-wave mixing term, while the two others are quadratic terms determining the effective inductance of modes X , Y and Z : $L_{X,Y,Z}^{-1} = \varphi_0^{-2} \partial^2 H / \partial \varphi_{X,Y,Z}^2$. The value $\varphi_{ext} = \pi/2$ maximizes the strength of the mixing term. Provided that

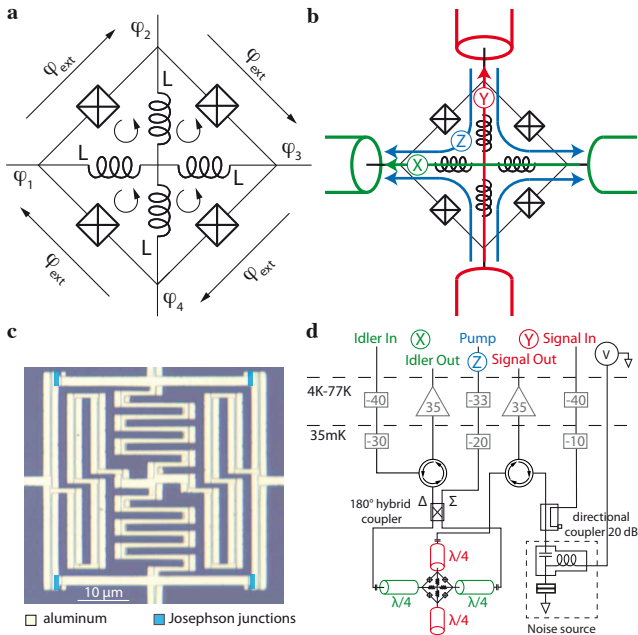


Figure 1: **a.** Device schematic: four linear inductances L cross-link a ring of four Josephson junctions. Each sub-loop is biased by a magnetic flux $\varphi_{ext}\varphi_0$. For $L < L_J^0/4$, the current through the inductances is zero and the external flux phase biases the junctions to φ_{ext} . **b.** The device is embedded at the intersection of four transmission lines and couples to spatial modes X , Y and Z represented as arrows. **c.** Optical microscope image of the ring modulator. The meanders in the center of the ring implement the four linear inductances from **a**. The stripes on the meanders are due to the fabrication process based on shadow evaporation. **d.** Simplified schematic of the setup used to characterize 3-wave mixing operation. The idler resonator (X) is excited through a 180° hybrid coupler while the signal resonator (Y) is single-ended. The noise emitted by the voltage biased tunnel junction in its normal state is amplified through the signal port.

$E_L/2 > E_J$, modes X and Y can be tuned by varying φ_{ext} while retaining their stability: $L_{X,Y}^{-1} > 0$ on the whole range of variation. However, there is a range of fluxes for which $L_Z^{-1} < 0$ where the device departs from $\langle \varphi_Z \rangle = 0$ so that the expansion (1) is inappropriate. If the inductances are lowered even more such that $E_L/4 > E_J$, then all three modes of the device are stable for every value of φ_{ext} , but at the expense of significant dilution of the non-linear term. In contrast, as E_L is lowered below $2E_J$, dilution of non-linearity is minimized, but at the expense of the stability of the three modes. This is why the JPC, for which $E_L = 0$, can operate only within a small range of values of φ_{ext} forbidding any tunability of the device.

We have tested this new, tunable, mixing element design, by inserting the ring into a resonant structure consisting of two $\lambda/2$ transmission line resonators coupled to the X and Y modes (Fig. 1d) as in Ref. [7]. The Z mode

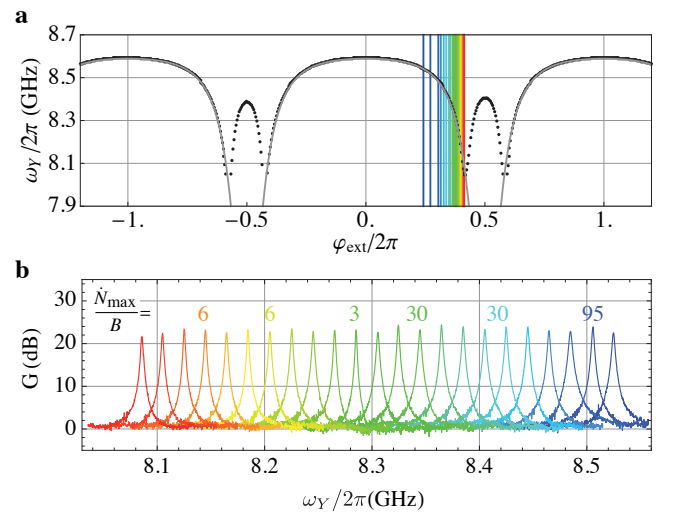


Figure 2: **a.** Dots: Measured resonance frequency ω_Y of the signal cavity as a function of flux applied to the ring modulator without pump. Solid line: fit of ω_Y using Eq. (2) with $\omega_Y^0/2\pi = 8.82$ GHz, $L = 49$ pH, $E_J = \varphi_0 \times 1.9$ μ A and including the known stray inductance around the loop $4L_S = 200$ pH (see ref.[9]). **b.** Reflection gain measured on the signal port as a function of frequency for various values of the flux indicated by the color lines in **a**. Pump parameters are optimized for each curve. The numbers on top represent the 1 dB compression point (maximum input power) expressed in input photon rate per dynamical bandwidth for six different working frequencies coded by color.

is non-resonant and excited through resonator X using a hybrid coupler (Fig. 1d). By varying the externally applied flux, it is possible to adjust the X and Y resonator frequencies given by

$$\omega_{X,Y} = \omega_{X,Y}^0 \frac{\pi^2 L_{X,Y}^{\lambda/2}/2}{\pi^2 L_{X,Y}^{\lambda/2}/2 + L_{X,Y}(\varphi_{ext})}, \quad (2)$$

where $\omega_{X,Y}^0$ is the resonance frequency of the bare $\lambda/2$ resonator without a ring, $L_{X,Y}^{\lambda/2} = 2Z_0/(\pi\omega_{X,Y}^0)$ its lumped-element equivalent inductance[1] and Z_0 its characteristic impedance. As long as $E_L/4 + E_J \cos \varphi_{ext} > 0$, the ring inductance $L_{X,Y}$ is given by

$$L_{X,Y}(\varphi_{ext}) = \varphi_0^2 \left(\frac{E_L}{2} + E_J \cos \varphi_{ext} \right)^{-1}. \quad (3)$$

The device presented in Fig. 1c is realized in a single e-beam lithography step. The critical current of the Al/Al₂O₃/Al Josephson junctions was designed to be in the μ A range. The wide geometric linear inductances cross-linking the ring are approximately given by $\mu_0 l$ where $l = 100$ μ m is the length of each of the four meanders. According to theory, they should present negligible kinetic inductance[8]. The value of the ratio

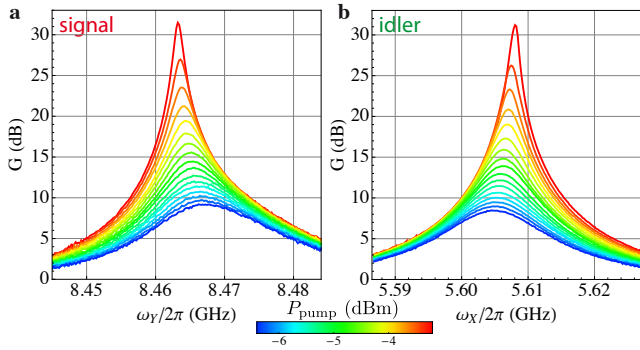


Figure 3: Reflection gain of the phase-preserving Josephson amplifier observed on the signal Y (a) and the idler X (b) modes. The color bar indicates the pump power referred to the output of the generator. The pump frequency is $\omega_Z/2\pi = 14.071$ GHz and the flux is set to $\varphi_{ext}/2\pi \approx 0.3125$.

$E_L/E_J = 3 \pm 2$ should favor the stability of the X and Y modes.

The device was operated in the photon gain mode. The phase and amplitude of the waves A_X^{out} and A_Y^{out} , relative to those of A_X^{in} and A_Y^{in} are measured with a vector network analyzer, for a whole set of pump tones A_Z^{in} . Turning off the pump tone first, we obtained the resonance frequency of both resonators as a function of flux (see Fig. 2a) as well as their half-maximum bandwidths $B_X = 39$ MHz and $B_Y = 29$ MHz. Unlike in the JPC, no hysteresis was found in the dependence of the resonance frequency on applied flux, confirming the stability of our device. However, two regimes must be distinguished in the data: that of the wide arches obeying (2) with a ring inductance given by (3) and that of the narrow arches for which $E_L/4 + E_J \cos \varphi_{ext} < 0$ and where the ring inductance depends precisely on the non-zero value of $\langle \varphi_Z \rangle$ emerging from the broken symmetry along the Z mode. It is interesting to note that the two possible opposite values for $\langle \varphi_Z \rangle$ in this regime give exactly the same resonance frequency. Besides, the fit of Fig. 2a does not take into account the perturbative effect of the parasitic inductances in series with the junctions. Using the full hamiltonian and these stray inductances, a complete agreement with the data can be obtained over the full flux variation range [9].

The power gain G of the device is defined as the ratio of the reflected power with pump on and off. The dependence of the gain on the pump power is shown on Fig. 3. Note in particular that a dynamical bandwidth $B = 3.2$ MHz is obtained for a gain of 20 dB. We checked that the parametric amplifier relation $\sqrt{G} \times B(G) = 2(B_X^{-1} + B_Y^{-1})^{-1}$ holds to less than a MHz of deviation for any pump power yielding a gain greater than 5 dB, for both signal and idler waves, as theory predicts [5].

As illustrated on Fig. 2b, the amplifier center frequency can be flux-tuned over 400 MHz which represents

a range two orders of magnitude greater than the bandwidth at 20dB. Indeed, for each center frequency, we can find a reproducible set of applied flux, pump power and pump frequency yielding a gain higher than 20 dB and a dynamical bandwidth of $B = 3$ MHz (Fig 2b). No amplification was found in the domain of the narrow arches. While this observation cannot be explained directly by the expansion (1), it is consistent with the full hamiltonian that predicts the non-linear term to be significantly spoiled by spurious terms when $\langle \varphi_Z \rangle \neq 0$. The key point of our experiment is that we can still benefit, outside the range of the narrow arches, from a comfortable tunable 3-wave non-linearity. The tunability of this non-degenerate amplifier can therefore compete with the state of the art degenerate Josephson amplifiers[10–15] with the added benefits of pump-signal separation.

We now turn to dynamical range measurements which further characterize the non-linear operation of our device. For these measurements, we first calibrated the attenuation of the line named "Signal In" (Fig. 1d) with an accuracy of 3 dB[16]. We then measured the so-called 1 dB compression point of the amplifier mode of our device, which is the input power for which the gain is reduced by 1 dB. As presented on Fig. 2b, this maximal power ranges between -133 dBm and -118 dBm, corresponding to 3 and 95 photons per inverse dynamical bandwidth. The reduction in maximal allowed power occurs at lower frequencies where we have also observed that the pump power needed for a given gain is ~ 30 dB lower than at higher frequencies. We believe that it could be explained by the pump frequency becoming, at lower signal frequencies, resonant with a mode of the crossed resonators. The device would hence depart from the stiff pump condition needed for parametric amplification with maximal dynamic range.

In a last series of experiments, the noise of our device was assessed by using the noise emitted by a voltage biased NIN tunnel junction as input signal. This noise, which is well-understood and therefore of predictable amplitude, plays the role of an *in situ* calibrated signal. At small electronic temperatures ($k_B T_e \ll \hbar \omega_S$), the noise from a tunnel junction presents two regimes as a function of voltage. For $eV < \hbar \omega_S$, zero-point fluctuations across the junction dominate with a power spectral density $S_p(\omega_S) = \frac{\hbar \omega_S}{2}$, while for $eV > \hbar \omega_S$, electrons in the junction produce non-equilibrium shot noise and $S_p(\omega_S) = \frac{eV}{2}$. The electronic temperature T_e in the electrodes of the junction sets the sharpness of the crossover between these two regimes [17, 18] as $S_p = S_p^+ + S_p^-$ with

$$S_p^\pm(\omega) = \frac{1}{4}(eV \pm \hbar\omega) \coth \frac{eV \pm \hbar\omega}{2k_B T_e}. \quad (4)$$

Our experiment was performed using an aluminum junction kept in its normal state by permanent magnets close-by. We measured *in situ* a normal resistance of

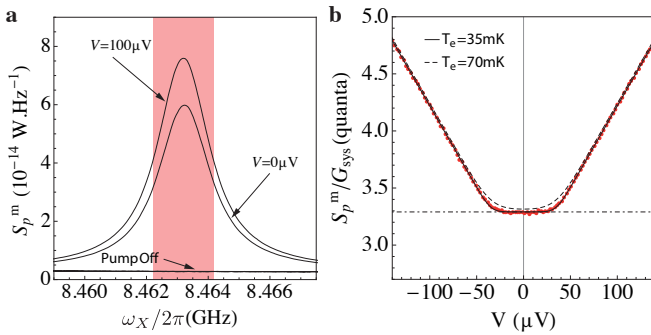


Figure 4: **a.** Power spectral density as a function of frequency measured at the output of "Signal Out" for three settings: pump *off* and $V = 0$, pump *on* and $V = 0$ or $V = 100 \mu\text{V}$. The colored area represents the averaging range used in the right panel. **b.** Average power spectral density over a 2 MHz bandwidth around the center frequency of the amplifier as a function of bias voltage V . The solid line shows what is expected using Eq. (5) and fitting an overall gain $G_{sys} = 94.6 \text{ dB}$ and an extra noise N_{add} of 2.8 quanta coming both from the unavoidable quantum noise of the idler port (0.5 quanta) and the unwanted losses between the tunnel junction and the amplifier (2.3 quanta). The gain G_{sys} allows us to express this power spectral density in units of photon number or quantum.

43.9Ω (measurement lines not shown on Fig. 1b). The output spectral density was recorded with a spectrum analyzer and averaged over a 2 MHz bandwidth around the center frequency of the amplifier (see Fig. 4a). Its dependence with bias voltage was obtained (Fig. 4b) for an amplifier gain of 23 dB with the same settings as in Fig. 3. The measured power spectral density is remarkably well described by an expression of the form:

$$S_p^m(\omega_S) = G_{sys}(S_p + N_{add} \hbar\omega_S). \quad (5)$$

In the shot noise regime, it is possible to calibrate the system gain $G_{sys} = dS_p^m/d(eV/2) = 94.6 \text{ dB}$ from the NIN tunnel element to the spectrum analyzer including a possible attenuation from the element to the input port of the amplifier. Without any additional calibration, we extracted the apparent system added noise $N_{add} = 2.8$ at the plateau (Fig. 4b). This number of quanta can be thought of as the standard half quantum attributable to the unavoidable quantum noise of the load at the idler port, and 2.3 quanta left which can be seen as an upper bound on the extra noise generated inside the device. On the other hand, an electronic temperature T_e equal to the refrigerator mixing chamber temperature of 35 mK describes perfectly the crossover. It is worth emphasizing that the noise power of the total measurement setup is presented in Fig. 4 without any background subtraction and is therefore the full *absolute* system noise. In fact, there is a finite attenuation between the junction and the amplifier leading to an underestimation of the gain counted from the input of amplifier and hence to the ac-

tual noise added by the device. Besides the unwanted insertion loss inherent to our type of low temperature measurement setup, the complex impedance of the junction itself is imperfectly matched[19]. Given the size of the junction ($\simeq 10 \mu\text{m}^2$) and previous experiments on similar junctions, we estimated its capacitance to be in the $0.7\text{pF} - 1 \text{ pF}$ range. Using the resistance of the junction and the characteristic impedance of the amplifier, we calculated that the loss of signal due to the RC filtering of the junction noise leads to an apparent added noise between 1.3 and 2.1 photons. Our measurement thus improves the N_{add} found by Bergeal *et al.* in that the measurement frequency and bandwidth are substantially higher[5]. It is straightforward to compare the noise measurement with and without our device. Turning off the pump tone, the same noise measurement using only a state-of-the-art HEMT amplifier at 4 K[20] yielded an apparent added noise 20 times larger than with the pump on. This translates into an acquisition time 400 times longer, keeping the same bandwidth.

In conclusion, we have shown that it is possible to realize with Josephson tunnel junctions a widely tunable, dissipation-less, non-degenerate 3-wave mixing element which processes microwave signals, adding a level of noise not significantly greater than the level of unavoidable quantum noise. Such an element could be useful in a certain number of analog quantum signal processing applications, like the feedback control of the state of a quantum bit[21].

Acknowledgments: Discussions with the Quantronics group at CEA Saclay, as well as with F. Mallet, F. Schackert and T. Kontos have been greatly useful. We gratefully acknowledge P. Pari and his team as well as O. Andrieu and J.C. Dumont for technical support. The devices have been made within the consortium Salle Blanche Paris Centre. We thank D. Maily for helping us dicing wafers at LPN-Marcoussis and the Quantronics group for metal evaporations. This work was supported by the EMERGENCES program Contract of Ville de Paris and by the ANR contract ULAMSIG.

* Present address: National Institute of Standards and Technology, 325 Broadway, Boulder CO 80305

† corresponding author: benjamin.huard@ens.fr

- [1] D. Pozar, *Microwave engineering* (J. Wiley, 2005).
- [2] M. Tinkham, *Introduction to superconductivity* (Dover Publications, 2004).
- [3] C. M. Caves, Phys. Rev. D **26**, 1817 (1982).
- [4] A. Clerk et al., Rev. Mod. Phys. **82**, 1155 (2010).
- [5] N. Bergeal et al., Nature (London) **465**, 64 (2010).
- [6] N. Bergeal et al., Nature Phys. **6**, 296 (2010).
- [7] B. Abdo et al., App. Phys. Lett. **99**, 162506 (2011).
- [8] A. J. Annunziata et al., Nanotech. **21**, 445202 (2010).
- [9] More details can be found in the EPAPS material:
- [10] M. A. Castellanos-Beltran et al., Nature Phys. **4**, 928

- (2008).
- [11] M. Hatridge et al., Phys. Rev. B **83**, 134501 (2011).
 - [12] T. Yamamoto et al., App. Phys. Lett. **93**, 042510 (2008).
 - [13] R. Vijay, D. H. Slichter, and I. Siddiqi, Phys. Rev. Lett. **106**, 110502 (2011).
 - [14] C. Eichler et al., Phys. Rev. Lett. **107**, 113601 (2011)
 - [15] C. M. Wilson et al., Phys. Rev. Lett. **105**, 233907 (2010)
 - [16] To calibrate the attenuation of the "Signal In" line, we first measure the amplification of the "Signal Out" line using the tunnel junction spectrum. We can then easily deduce the attenuation at the input by measuring the transmission from "Signal In" to "Signal Out" lines over a wide range of powers. A 3 dB uncertainty remains due to the imperfectly known impedance of the tunnel junction.
 - [17] R. J. Schoelkopf et al., Phys. Rev. Lett. **78**, 3370 (1997).
 - [18] Y. Blanter and M. Buttiker, Phys. Rep. **336**, 1 (2000).
 - [19] L. Spietz et al., App. Phys. Lett. **97**, 142502 (2010).
 - [20] S. Weinreb, M. W. Pospieszalski, and R. Norrod, Microwave Symposium Digest, IEEE MTT-S International **2** 945 (1988).
 - [21] A. Korotkov, Phys. Rev. B **71**, 201305 (2005)